minerals

MDPI

Article

Equations of State of Ca-Silicates and Phase Diagram of the $CaSiO_3$ System under Upper Mantle Conditions

Tatiana S. Sokolova * and Peter I. Dorogokupets

Institute of the Earth's Crust, Siberian Branch of the Russian Academy of Sciences, 664033 Irkutsk, Russia; dor@crust.irk.ru
* Correspondence: sokolovats@crust.irk.ru; Tel.: +7-39-5251-1680

Abstract: The equations of state of different phases in the $CaSiO_3$ system (wollastonite, pseudowollastonite, breyite (walstromite), larnite (Ca_2SiO_4), titanite-structured $CaSi_2O_5$ and $CaSiO_3$-perovskite) are constructed using a thermodynamic model based on the Helmholtz free energy. We used known experimental measurements of heat capacity, enthalpy, and thermal expansion at zero pressure and high temperatures, and volume measurements at different pressures and temperatures for calculation of parameters of equations of state of studied Ca-silicates. The used thermodynamic model has allowed us to calculate a full set of thermodynamic properties (entropy, heat capacity, bulk moduli, thermal expansion, Gibbs energy, etc.) of Ca-silicates in a wide range of pressures and temperatures. The phase diagram of the $CaSiO_3$ system is constructed at pressures up to 20 GPa and temperatures up to 2000 K and clarifies the phase boundaries of Ca-silicates under upper mantle conditions. The calculated wollastonite–breyite equilibrium line corresponds to equation $P(\text{GPa}) = -4.7 \times T(\text{K}) + 3.14$. The calculated density and adiabatic bulk modulus of $CaSiO_3$-perovskite is compared with the PREM model. The calcium content in the perovskite composition will increase the density of mineral and it good agree with the density according to the PREM model at the lower mantle region.

Keywords: equation of state; the Helmholtz free energy; thermodynamic properties; $CaSiO_3$; wollastonite; breyite; perovskite; phase transition; diamond; mantle

Citation: Sokolova, T.S.; Dorogokupets, P.I. Equations of State of Ca-Silicates and Phase Diagram of the $CaSiO_3$ System under Upper Mantle Conditions. *Minerals* **2021**, *11*, 322. https://doi.org/10.3390/min11030322

Academic Editor: Fumagalli Patrizia

Received: 29 January 2021
Accepted: 16 March 2021
Published: 19 March 2021

1. Introduction

The thermodynamic description and phase equilibria in the $CaSiO_3$ system are important for modern mineralogical research because Ca-silicates are common components of the Earth's crust and mantle. The low-pressure $CaSiO_3$ polymorphs (wollastonite and pseudowollastonite) are rock-forming minerals in the Earth's crust and constitute cement substances [1,2], while the high-pressure Ca-silicate phases (breyite (walstromite), larnite, titanite-structured $CaSi_2O_5$ and $CaSiO_3$-perovskite) are stable in the mantle P-T conditions and detected as solid-phase inclusions in natural diamonds [3–7]. The presence of $CaSiO_3$ phase in diamonds indicates the possibility of transporting the substance from the lower mantle to the surface in an unchanged form and provides insights into the nature of diamond formation. Thus, the present study will expand the possibility for thermodynamic modeling of physicochemical processes in the Earth's deep mantle.

It is well known that calcium metasilicate ($CaSiO_3$) has a number of structural modifications at relevant pressures and temperatures. Wollastonite structure is stable under ambient conditions and transforms to pseudowollastonite phase at high temperatures above ~1400 K [8]. The transition of wollastonite to walstromite-structured $CaSiO_3$ is detected at 3 GPa and 1173 K [9]. The name breyite for this phase is approved by IMA in 2018 [10], therefore it is used in the text below. The wollastonite–breyite equilibrium was studied by different authors [1,11,12]. The subsequent decomposition of breyite to association of larnite (Ca_2SiO_4) and titanite-structured $CaSi_2O_5$ was determined at higher pressures by Kanazaki's study [13]. The $CaSiO_3$-perovskite is formed at pressure ~14 GPa from (larnite + $CaSi_2O_5$) assemblage [14] and retains its structure until lower mantle conditions. The phase diagram of the $CaSiO_3$ is well studied at low pressures up to 3–4 GPa and high temperatures by experimental methods in [11,15]. In the present calculation, we also used the phase diagram of the $CaSiO_3$ system, which was proposed in [1,11].

The thermodynamics of Ca-silicates can be calculated from their equations of state (EoS). The equations of state of wollastonite, pseudowollastonite, breyite, larnite (Ca_2SiO_4), titanite-structured $CaSi_2O_5$ and $CaSiO_3$-perovskite can be constructed based on the thermodynamic model, which was successfully used in our previous studies for the $MgSiO_3$–MgO system [16,17]. We use a thermodynamic model based on the Helmholtz free energy, which allows us to calculate a full set of thermodynamic properties (entropy, heat capacity, bulk moduli, thermal expansion, Gibbs energy, etc.) at given P-T or V-T parameters. The proposed thermodynamic model is based on optimization of different experimental measurements (dilatometric, X-ray diffraction, ultrasonic interferometry, etc.) and theoretical data (calculations and reference) by analogy with our studies for metals [18–20] and compounds [21,22]. The proposed equations of state of studied Ca-silicates are constructed with a small number of fitting parameters. There are also other different forms of EoSes, which contain a small number of parameters and reliably describe the properties of metals and mixtures [23–26], but in this study, we will use our model that previously showed its versatility.

2. Thermodynamic Model

The equations of state of wollastonite, pseudowollastonite, breyite, larnite (Ca_2SiO_4), titanite-structured $CaSi_2O_5$ and $CaSiO_3$-perovskite are constructed using the thermodynamic model based on the Helmholtz free energy. According to the proposed thermodynamic model, the Helmholtz free energy can be represented in general form as the sum [27]:

$$F(V,T) = \mathcal{U}_0 + F_{T_0}(V) + F_{th}(V,T) + F_{anh}(V,T), \tag{1}$$

where U_0 is the reference energy, F_{T0} is the potential part of the Helmholtz free energy at the reference isotherm T_0 = 298.15 K, which depends only on volume; F_{th} is the thermal part of the Helmholtz free energy, which depends on volume and temperature; F_{anh} is an additional contribution to the Helmholtz free energy, which connects with intrinsic anharmonicity, as a function of temperature and volume.

The potential part of the Helmholtz free energy from Equation (1) is determined by the integration of the equation of pressure at the reference isotherm. Many different equations are known to express the equation of pressure at the reference isotherm, each of which has its advantages and limitations (review in [17]). We use the Kunc equation [28], which is flexible in calculations because it contains parameter k:

$$P_{T_0}(V) = 3K_0X^{-k}(1-X)\exp[\eta(1-X)], \tag{2}$$

where $X = (V/V_0)^{1/3}$, $\eta = 1.5K' - k + 0.5$, K_0 is the isothermal bulk modulus under ambient conditions (P_0 = 1 bar = 10^{-4} GPa, T_0 = 298.15 K), $K' = \partial K_0/\partial P_0$ and k is an additional parameter.

When $k = 2$, the Kunc equation corresponds to the Vinet equation [29], which is often used in calculation of equations of state of metals in solid state physics. The values of $k = 5$ and $k > 5$ transform the Kunc equation into one of the forms of the Holzapfel equation (HO_2) [30] and into the Birch–Murnaghan equation [31], respectively. We use $k = 5$ for all Ca-silicate phases in the present study.

Differentiating Equation (2) with respect to volume at constant temperature, we determine the isothermal bulk modulus at the reference isotherm and calculate of its derivation by pressure:

$$K_{T0}(V) = -V\left(\frac{\partial P_{T_0}}{\partial V}\right)_T = K_0X^{-k}\exp[\eta(1-X)][X + (1-X)(\eta X + k)], \tag{3}$$

$$K'(V) = \left(\frac{\partial K_{T0}}{\partial P_{T_0}}\right) = \frac{1}{3}\left[k + \eta X + \frac{kX + 2X^2\eta - X(1+\eta)}{X + (1-X)(\eta X + k)}\right]. \tag{4}$$

The thermal part of the Helmholtz free energy from Equation (1) can be calculated by Debye, Einstein, Bose–Einstein models, or their combinations [32,33]. A more simple approach is to use the Einstein model with two characteristic temperatures, which makes it possible to good approximate of the heat capacity in the temperature range from ~100 K to the melting point of the substance:

$$F_{th}(V,T) = \sum_{i=1,2} m_i RT \ln\left(1 - \exp\frac{-\Theta_i}{T}\right), \tag{5}$$

where m_i is proportionality factor, which is calculated from the total number of atoms in the compound (i = 1, 2), m_1 + m_2 = 3n, n is the number of atoms in a chemical formula of the compound, Θ_i is the Einstein characteristic temperature, which depends only on volume, and R is the gas constant (R = 8.31451 Jmol^{-1}K^{-1}).

The volume dependence of characteristic temperature in Equation (5) is determined by Al'tshuler equation [34]:

$$\Theta_i = \Theta_{0i} x^{-\gamma_\infty} \exp\left[\frac{\gamma_0 - \gamma_\infty}{\beta}\left(1 - x^\beta\right)\right], \tag{6}$$

where Θ_{0i} is the characteristic temperature under ambient conditions (i = 1, 2), $x = V/V_0$, γ_0 is the Grüneisen parameter at ambient conditions, γ_∞ is the Grüneisen parameter at infinite compression, when $x \to 0$, and β is an additional fitting parameter.

The advantage of Equation (6) is that it can be explicitly differentiated in the simple form to determine the Grüneisen parameter:

$$\gamma = -\left(\frac{\partial \ln \Theta}{\partial \ln V}\right)_T = \gamma_\infty + (\gamma_0 - \gamma_\infty)x^\beta, \tag{7}$$

where Θ is the characteristic temperature in general case.

We assume that the Grüneisen parameter will be the same for both characteristic temperatures (Θ_1 and Θ_2) in Equation (6). In addition, if γ_∞ = 0, then Equation (7) transforms to the classical form $\gamma = \gamma_0 x^\beta$.

Differentiating Equation (5) with respect to temperature at constant volume, we determine entropy and then calculate internal energy:

$$S = -\left(\frac{\partial F_{th}}{\partial T}\right)_V = \sum_{i=1,2} 3nR\left[-\ln\left(1 - \exp\frac{-\Theta_i}{T}\right) + \frac{\Theta_i/T}{\exp(\Theta_i/T) - 1}\right], \tag{8}$$

$$E_{th} = F_{th} + TS = \sum_{i=1,2} 3nR\left[\frac{\Theta_i}{\exp(\Theta_i/T) - 1}\right]. \tag{9}$$

Differentiating Equation (5) with respect to volume at constant temperature, we obtain the thermal part of pressure:

$$P_{th} = -\left(\frac{\partial F_{th}}{\partial V}\right)_T = \sum_{i=1,2} 3nR\frac{\gamma}{V}\left[\frac{\Theta_i}{\exp(\Theta_i/T) - 1}\right] = \frac{\gamma}{V}E_{th}. \tag{10}$$

Differentiating Equation (9) with respect to temperature at constant volume and Equation (10) with respect to volume at constant temperature, we obtain the isochoric heat capacity and thermal part of isothermal bulk modulus:

$$C_V = \left(\frac{\partial E_{th}}{\partial T}\right)_V = \sum_{i=1,2} 3nR\left(\frac{\Theta_i}{T}\right)^2 \frac{\exp(\Theta_i/T)}{(\exp(\Theta_i/T) - 1)^2}, \tag{11}$$

$$K_{Tth} = -V\left(\frac{\partial P_{th}}{\partial V}\right)_T = P_{th}(1+\gamma-q) - \gamma^2 C_V \frac{T}{V}, \tag{12}$$

where q is additional parameter, which is calculated from Equation (7) according to [34].

Differentiating Equation (10) with respect to temperature at constant volume, we determine the slope:

$$(\partial P_{th}/\partial T)_V = \frac{\gamma}{V} C_V. \tag{13}$$

The additional contribution of the intrinsic anharmonicity to the Helmholtz free energy in Equation (1) can be expressed by classical equation from [27]:

$$F_{anh}(V,T) = -\frac{3}{2}nRaT^2 = -\frac{3}{2}nRa_0x^mT^2. \tag{14}$$

The contribution of the intrinsic anharmonicity to entropy, internal energy, thermal part of pressure, isochoric heat capacity, thermal part of isothermal bulk modulus and slope can be obtained by analogy with Equations (8)–(13), respectively:

$$\begin{aligned} S_{anh} &= 3nRaT, \\ E_{anh} &= \tfrac{3}{2}nRaT^2, \\ C_{V_{anh}} &= 3nRaT, \\ P_{anh} &= \tfrac{3}{2}nRa\tfrac{m}{V}T^2 = \tfrac{m}{V}E_{anh}, \\ K_{T_{anh}} &= P_{anh}(1-m), \\ (\partial P_{anh}/\partial T)_V &= \tfrac{m}{V}C_{V_{anh}}, \end{aligned} \tag{15}$$

where $a = a_0x^m$, a_0 is the intrinsic anharmonicity parameter and m is the anharmonic analogue of the Grüneisen parameter.

The Equation (10) for the thermal part of pressure and equation for anharmonicity part of pressure (P_{anh} in Equation (15)), as can be seen, are very similar. The Grüneisen parameter in Equation (10) is the coefficient of proportionality between pressure and internal energy, just like the parameter m in Equation (15). Therefore, we use this name for the parameter m. The parameters a_0 and m are fitting parameters in the general cause, but we use the fixed value for m ($m = 1$) in the present study.

The full equations of pressure and isothermal bulk modulus are calculated as the sum of potential, thermal, and anharmonicity components: $P = P_{T0}(V) + P_{th}(V,T) + P_{anh}(V,T)$ and $K_T = K_{T0}(V) + K_{Tth}(V,T) + K_{Tanh}(V,T)$. Further, it is easy to calculate the coefficient of thermal expansion $\alpha = (\partial P_{th}/\partial T)_V / K_T$, the heat capacity at constant pressure $C_P = C_V + \alpha^2 TVK_T$, the adiabatic bulk modulus $K_S = K_T + VT(\alpha K_T)^2/C_V$, and the thermodynamic Grüneisen parameter $\gamma_{th} = \alpha VK_T/C_V = \alpha VK_S/C_P$. The enthalpy and Gibbs energy are determined from the linear relations $H = E_{th} + PV - P_0V_0$ and $G = F(V,T) + PV - P_0V_0$, respectively. The parameter U_0 in Equation (1) define the Gibbs energy under ambient conditions, which also can be found from the simple relation: $U_0 = \Delta G_{f,298} = \Delta H_{f,298} - S_{298}T_0$, where $\Delta H_{f,298}$ and S_{298} are enthalpy and entropy at ambient conditions, respectively.

Thus, Equations (1)–(15) contain a group of fixed parameters (V_0, k, m_i) and a group of fitting parameters (K_0, K', Θ_{0i}, γ_0, γ_∞, β, a_0, m) derived by least squares method in Excel worksheet. Using the proposed approach, it is easy to calculate a full set of thermodynamic functions of Ca-silicates that depend on temperature, pressure, and volume.

3. Results

The equations of state of studied Ca-silicates were constructed using thermodynamic model described above. Table 1 shows parameters of equations of state for wollastonite (Wol), pseudowollastonite (PsWol), breyite (Brt), larnite (β-Lrn), titanite-structured $CaSi_2O_5$ (Ca-Tit) and $CaSiO_3$-perovskite (Ca-Pv) obtained by simultaneous optimization of known thermochemical measurements of the heat capacity, enthalpy, thermal expansion, and numerous *P*-*V*-*T* data including modern X-ray diffraction measurements for the Ca-silicate minerals. The optimization procedure is described in detail in our previous works [16,20,33]. In the present study, we also offer the open working MS Excel spreadsheets for each of the studied Ca-silicates (Files S1–S6 in Supplementary Material). Detailed instructions and descriptions of worksheets are provided in [17,19]. Therefore, below we will focus on the features of calculating of equation of state for each of the phases.

Table 1. Parameters of equations of state of Ca-silicates at ambient conditions.

Parameters	**Wol** **$CaSiO_3$**	**PsWol** **$CaSiO_3$**	**Brt $CaSiO_3$**	**β-Lrn** **Ca_2SiO_4**	**Ca-Tit** **$CaSi_2O_5$**	**Ca-Pv** **$CaSiO_3$**
$\mathcal{U}_0$, kJmol^{-1}	−1658.007	−1655.531	−1651.400	−2344.025	−2524.000	−1567.400
V_0, cm^{3}mol^{-1}	39.9	40.3	37.78	51.88	48.19	27.403
K_0, GPa	81.5	86	78.6	105	178	239
K'	3.28	3.8	4	6.27	4	4.13
k	5	5	5	5	5	5
Θ_{01}, K	966	1039	952	838	975	935
m_1	7.5	7.5	7.5	10.5	12	7.5
Θ_{02}, K	270	244	280	257	370	388
m_2	7.5	7.5	7.5	10.5	12	7.5
γ_0	1	1	0.745	1.263	1.3	1.913
γ_∞	0	0	0	0	0	0
β	1	1	1	1.041	1	0.486
a_0, 10^{-6} K^{-1}			20.8			
m			1			

Wollastonite (Wol). A review of the heat capacity measurements of wollastonite and other $CaSiO_3$ phases can be found in [35]. The most reliable measurements we found of molar volume of wollastonite as a function of temperature are published in [36]. The only known measurement of the volume of wollastonite as a function of pressure in [37] shows the following values of K_0 = 54.7 GPa and $\partial K/\partial P$ = 23.5. However, at these values, our equation of state of wollastonite becomes unstable at temperatures above 700 K (this is easily verified by substituting the parameters to the present Excel file for wollastonite). Therefore, we use measurements of volume, depending on pressure for pseudowollastonite from [38]. The simultaneous optimization of known experimental data for wollastonite at $\gamma_0 = 1$, $\beta = 1$ and $\gamma_\infty = 0$ determine the obtained parameters of its equation of state (Table 1). Figure 1a shows a comparison of the calculated isobaric (C_P) and isochoric (C_V) heat capacity of wollastonite with measurements from [39–42]; Figure 1c shows calculated molar volume at reference pressure (P_0 = 1 bar = 10^{-4} GPa) with Swamy's data [36]; and Figure 1e shows calculated compressibility as a function of pressure with measurements from [37]. It can be seen that calculated data are in good agreement with different reference and experimental data.

The calculated thermodynamic functions of wollastonite at different temperatures and pressures (0.0001 and 3 GPa) are presented in Table 2. The last column shows the Gibbs energy at given *P*-*T* parameters. The parameter U_0 is calculated from the enthalpy at ambient conditions $\Delta H_{f,298}$ = −1633.750 kJmol^{-1} from [43] and entropy S_{298} = 81.358 Jmol^{-1} K^{-1} at ambient conditions from Table 2, then $U_0 = \Delta G_{f,298} = -1{,}633{,}750 - 81.358 \times 298.15 = -1{,}658{,}007$ Jmol^{-1}. The same scheme was used for calculation of the Gibbs energy for Mg-silicates in the Mg_2SiO_4 system [16]. We have shown calculation thermodynamic functions for wollastonite in the Table 2. Further tabulated values of calculated thermodynamic functions for other Ca-silicates are presented in the Supplementary Material (Tables S1–S5).

Table 2. Thermodynamic functions of wollastonite at different pressures and temperatures.

***P*, GPa**	***T*, K**	***V*, cm^3 mol^{-1}**	**$\alpha \times 10^6$, K^{-1}**	***S*, Jmol^{-1} K^{-1}**	**C_P, Jmol^{-1} K^{-1}**	**C_V, Jmol^{-1} K^{-1}**	**K_T, GPa**	**K_S, GPa**	**ΔG, kJmol^{-1}**
0.0001	298.15	39.900	26.458	81.358	86.715	86.037	81.50	82.14	−1658.007
0.0001	500	40.147	33.714	132.366	108.976	107.159	79.66	81.01	−1679.826
0.0001	1000	40.907	40.288	214.108	124.900	119.946	74.62	77.70	−1768.341
0.0001	1398	41.596	43.519	256.827	130.068	122.310	70.44	74.91	−1862.474
0.0001	2000	42.763	48.446	304.482	136.431	123.596	63.94	70.58	−2032.169
3	298.15	38.536	23.175	78.447	84.890	84.327	91.20	91.81	−1540.406
3	500	38.746	29.732	128.623	107.621	106.089	89.43	90.72	−1561.542
3	1000	39.393	35.446	209.562	123.771	119.586	84.55	87.51	−1647.956
3	1500	40.130	38.619	260.949	129.599	122.464	79.48	84.11	−1766.352
3	2000	40.944	41.668	298.850	134.050	123.490	74.28	80.63	−1906.702

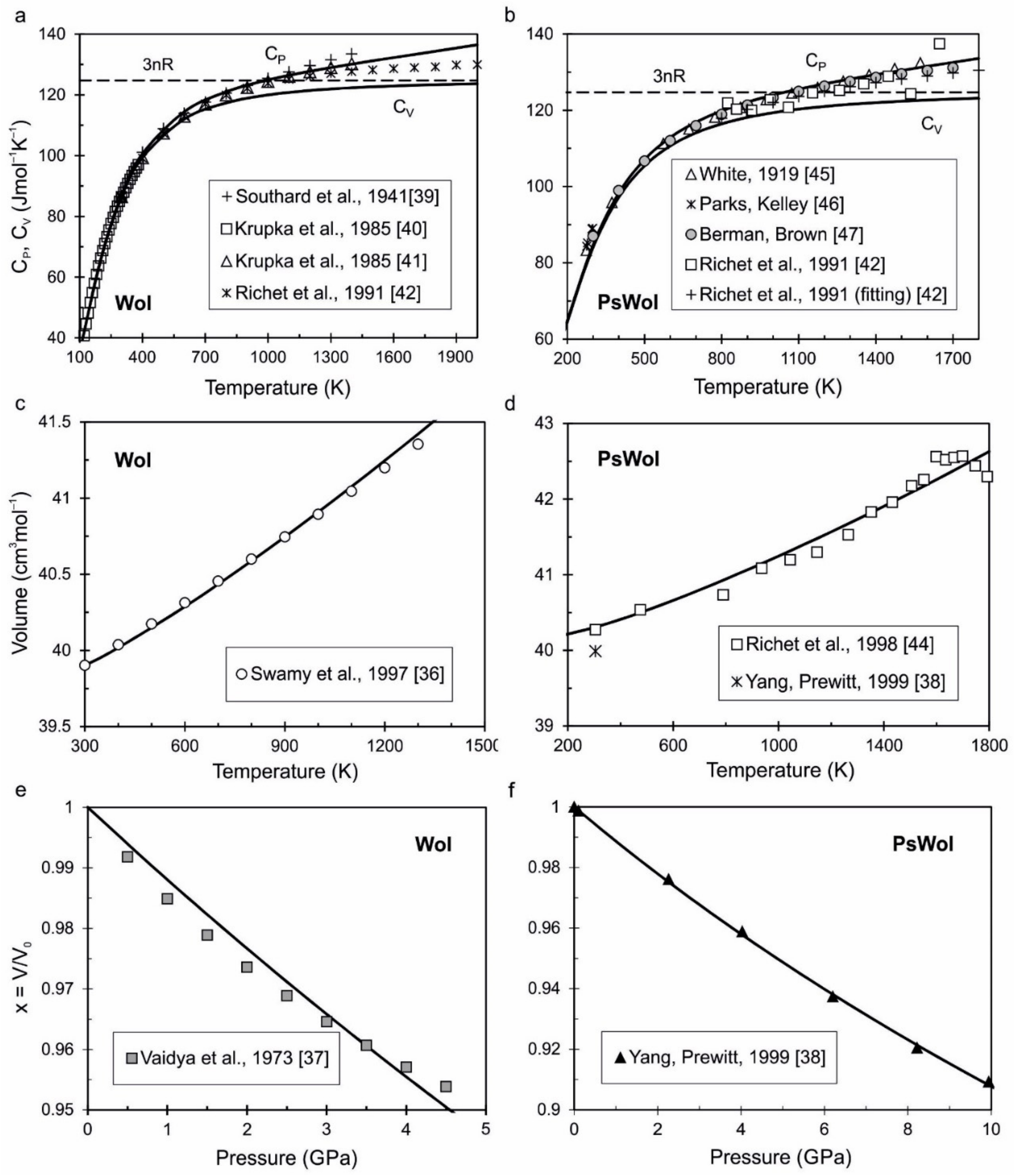

Figure 1. The calculated heat capacity (**a**,**b**), molar volume at reference pressure (**c**,**d**) and compressibility as a function of pressure (**e**,**f**) of wollastonite (Wol) and pseudowollastonite (PsWol) in comparison with different reference and experimental data from [36,37,39–42] for Wol and from [38,42,44–47] for PsWol.

Pseudowollastonite (PsWol). As follows from the review in [2], wollastonite at ambient conditions has a triclinic structure (space group $P1$). The crystal structure of a synthetic two-layer polytype of pseudowollastonite was studied using single-crystal X-ray diffraction data at pressures up to 10 GPa by Yang and Prewitt [38]. It is determined that such a polytype has monoclinic structure (space group $C2/c$) and molar volume at ambient condition (V_0 = 796.9 A^3 = 39.99 cm^{3}mol^{-1}) coincides with the volume of wollastonite (Table 2). The molar volume of pseudowollastonite was studied at temperature range 307–1793 K by Richet et al. [44]. There are two-, four-, and six-layer polytypes of CaSiO$_3$-pseudowollastonite in this temperature range. The parameters of K_0 and K' for our calculation were extracted from [38]; parameters of Θ_{01} and Θ_{02} are calculated from the heat capacity and relative enthalpy measurements from [42,45–47]. The parameter U_0 is calculated from the condition of equality of the Gibbs energy of wollastonite and pseudowollastonite at T = 1398 K and P = 0.0001 GPa.

The difference of calculated entropy at 1398 K for wollastonite–pseudowollastonite transition is ΔS_{1398} = 1.586 $\mathrm{Jmol^{-1}K^{-1}}$ (see Table 2 and Table S1), while in Richet's study, it is $\Delta S_{1398} = 4.2 \pm 2$ $\mathrm{Jmol^{-1}K^{-1}}$ [42]. However, taking into account ΔV_{1398} = 0.3036 $\mathrm{cm^3mol^{-1}}$, we obtain the slope $\partial P/\partial T = \Delta S/\Delta V = 52.2 \times 10^{-4}$ GPa/K, which is in good agreement with data from [11,48].

The calculated thermodynamic functions of pseudowollastonite are compared with different reference and experimental data [38,44] by analogy with wollastonite on Figure 1b,d,f. The tabulated values of calculated thermodynamic functions of pseudowollastonite as a function of temperature at different pressures (0.0001 and 3 GPa) is presented in the Supplementary Material (Table S1).

Breyite (Brt). Regarding of breyite, in the literature, we can find the different names of its structural isomorphs (Ca-walstromite, wollastonite-II, walstromite-like $CaSiO_3$(III)). The crystal structures of breyite (or walstromite), $CaSiO_3$-walstromite, and wollastonite-II are very similar. This issue is discussed in detail by Joswig et al. [49]. Breyite probably crystallizes in the triclinic structure (space group $P1$) and it is stable in the pressure range from ~3 GPa and above, since the remaining pressure of investigated inclusions of breyite in natural diamonds [3,4] was also estimated to be 3 GPa. The direct P-V-T measurements of breyite are carried out in [5,50]. The parameters of V_0, K_0 and K' are taken from Anzolini et al. [5]. The parameter U_0 is calculated from the phase transition of wollastonite–breyite. The calculated volume of breyite as a function of temperature and pressure is compared with experimental data on Figure 2a,b. The tabulated values of calculated thermodynamic functions of breyite depending on temperature at different pressures (0.0001, 5 and 10 GPa) is presented in the Supplementary Material (Table S2).

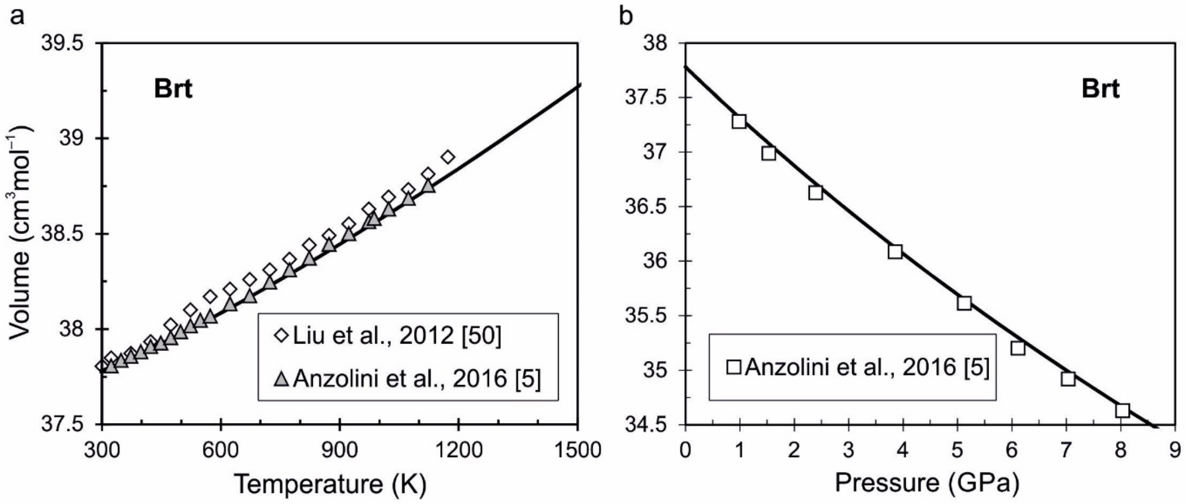

Figure 2. The calculated volume of breyite as a function of temperature (**a**) and pressure (**b**) is compared with experimental data from [5,50].

Larnite (β-Lrn). As temperature increases, the composition of Ca_2SiO_4 can form a series of polymorphs (γ-, β-, α'_L-, α'_H- and α). The review of crystal structures of Ca_2SiO_4 is presented for example in [51,52]. The β-larnite is formed as metastable monoclinic phase (space group $P2_1/n11$) in the stability field of γ-Ca_2SiO_4 by its cooling. We considered here only the beta modification, which is typical for natural larnite [53]. Larnite (β phase) has a wide stability field at high pressures and temperatures; therefore, this phase is used in the present study. The parameter V_0 is taken from Remy et al. [51], and other parameters (K_0, K', Θ_{0i}, γ_0, γ_∞ and β) are calculated from optimization of experimental measurements of heat capacity and P-V-T data from [51,54–57]. The parameter U_0 is calculated from the enthalpy at ambient conditions $\Delta H_{f,298} = -2307.04$ $\mathrm{kJmol^{-1}}$ from [43] and entropy at ambient conditions S_{298} = 124.047 $\mathrm{Jmol^{-1}K^{-1}}$ from Table S3 (Supplementary Material). The other tabulated values of calculated thermodynamic functions of larnite depending on temperature at different pressures (0.0001, 10 and 15 GPa) is presented also in Table S3.

The calculated volume of larnite as a function of pressure and temperature is compared with experimental data on Figure 3a,b.

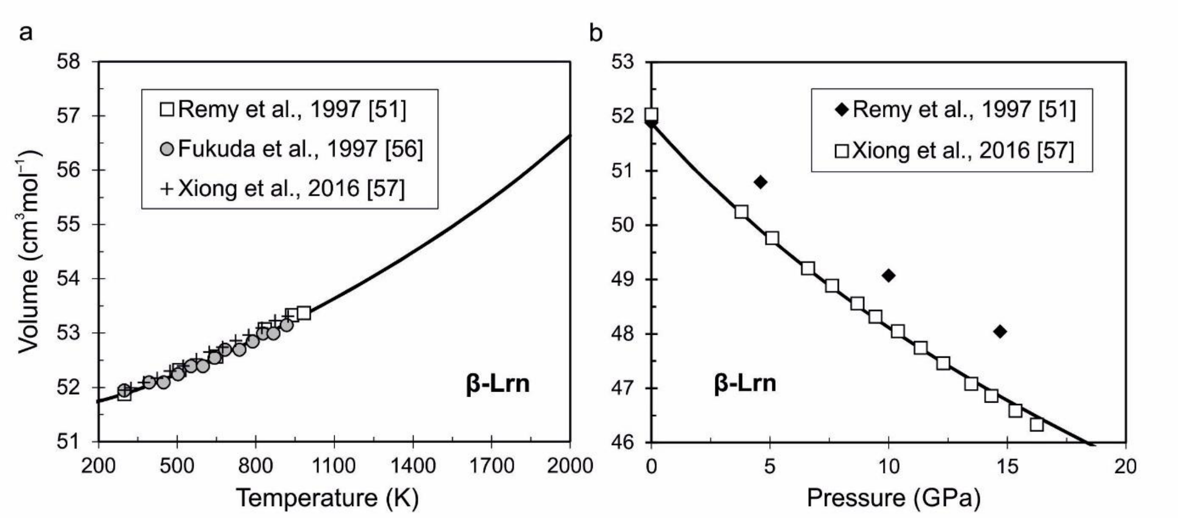

Figure 3. The calculated volume of larnite (β phase) as a function of temperature (**a**) and pressure (**b**) is compared with experimental data from [51,56,57].

Titanite-structured $CaSi_2O_5$ (Ca-Tit). The titanite-structured $CaSi_2O_5$ phase is identified by in situ XRD analyses in natural diamonds from Guinea and Brazil [3–5], but thermochemical data for this phase are not available. Therefore, the present equation of state of titanite-structured $CaSi_2O_5$ (space group $C2/c$) is constructed on the values of parameters of V_0, K_0 and K' from [58], and other parameters (Θ_{0i}, γ_0, γ_∞ and β) are calculated from optimization of experimental data from [2,58]. The parameter U_0 for Ca-titanite is calculated from values of enthalpy and entropy at ambient conditions with analogy for wollastonite and larnite calculations. The tabulated values of calculated thermodynamic functions of titanite-structure $CaSi_2O_5$ as a function of temperature at different pressures (0.0001, 10 and 15 GPa) is presented in the Supplementary Material (Table S4).

Perovskite (Ca-Pv). $CaSiO_3$-perovskite is considered as the one of the main Ca-bearing phase in the Earth's lower mantle [59]. Therefore, findings of Ca-perovskite in natural diamond [6] may explain the mechanisms of diamond formation in general. The question of nature of "super-deep" diamond is discussed widely; however, the aim of this study is to reliably calculate the thermodynamic functions of $CaSiO_3$-perovskite in a wide range of pressures and temperatures. $CaSiO_3$-perovskite is stabilized in the cubic structure (space group $Pm3m$) at temperatures above 1000 K and pressures above 11–16 GPa, according to [1]. At low temperatures up to 500 K and high pressures up to 156 GPa, the $CaSiO_3$-perovskite has a distorted cubic structure, which is identified in [60,61] as tetragonal modification (space group $I4/mcm$). The direct measurements of heat capacity and bulk modulus as a function of temperature at ambient pressure for cubic Ca-perovskite are not available [62]; therefore, all parameters (K_0, K', Θ_{0i}, γ_0, γ_∞ and β) for proposed equation of state were calculated by authors. However, numerous experimental measurements of molar volume of Ca-perovskite at different pressures and temperatures are known (Table 3). The proposed equation of state of $CaSiO_3$-perovskite is constructed on the modern P-V-T measurement from [60,61,63] and simultaneous sound velocities and density measurements at pressures up to 23 GPa and temperatures up to 1700 K from [64]. The pressure measurements in [63] were recalculated based on the equation of state of Pt from [65]; the pressure from [60] was calculated using a self-consistent pressure scale of Pt from [66]; and pressure from [64] was monitored during the experiment by the unit-cell volume of NaCl [67].

Table 3. Direct experimental measurements of molar volume of $CaSiO_3$-perovskite.

Pressure Range, GPa	Temperature Range, K	Method	Reference
0–134	300	XRD	[68]
16.8–108	300	XRD	[69]
28–62	300	XRD	[61]
0.59–13	301–1600	XRD	[70]
18–96	1238–2419	XRD	[71]
51–130	700–2300	XRD	[63]
21.2–156	1200–2600	XRD	[60]
12–23	700–1700	XRD	[64]

The differences in measurements of volume in Table 3 are significant, so the proposed equation of state of Ca-perovskite here is important. Figure 4a,b shows the deviations of the experimental measured pressure in [60,63] and calculated pressure from the proposed equation of state. It can be seen that the most differences are observed at pressure over 100 GPa. Figure 5a,b shows a difference between calculated pressure and adiabatic bulk modulus and experimental data from [64]. The tabulated values of calculated thermodynamic functions of cubic $CaSiO_3$-perovskite as a function of temperature at different pressures (0.0001, 10, 15 and 100 GPa) are presented in the Supplementary Material (Table S5).

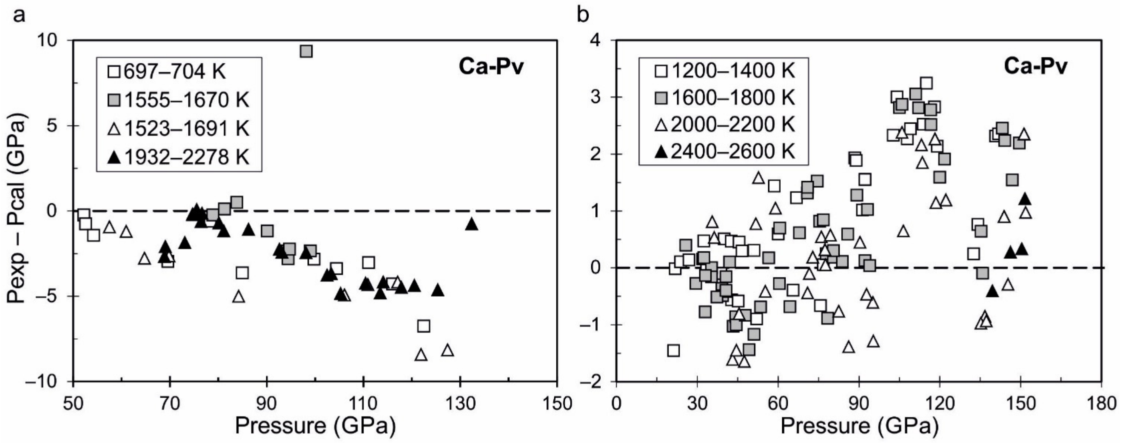

Figure 4. Difference between experimental measured pressure in [63] (**a**) and in [60] (**b**) and calculated pressure from the proposed equation of state of Ca-perovskite at different isotherms. The pressure in [63] is recalculated from the equation of state of Pt [65]; pressure in [60] is determined using the equation of state of Pt [66].

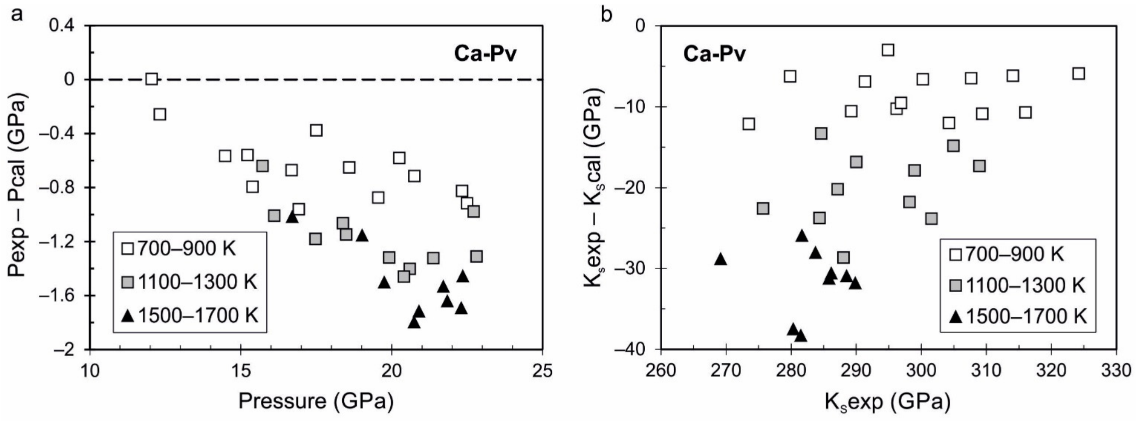

Figure 5. Difference between experimental measured pressure (**a**) and adiabatic bulk modulus (**b**) from [64] and calculated pressure and adiabatic bulk modulus from the proposed equation of state of Ca-perovskite. The pressure in [64] is calculated from the equation of state of NaCl [67].

4. Discussion

The proposed equations of state of wollastonite, pseudowollastonite, breyite (walstromite), larnite, titanite-structured $CaSi_2O_5$ and $CaSiO_3$-perovskite allow us to calculate the phase diagram of the $CaSiO_3$ system (Figure 6). The wollastonite–pseudowollastonite equilibrium corresponds to the data from [11,48], which were used for calibration of the Gibbs energy of pseudowollastonite. At a pressure of about 3 GPa and temperature of about 1100 K wollastonite transforms to breyite (walstromite). The Gibbs energy of breyite is calibrated based on measurements from [11,15]. The calculated wollastonite–breyite equilibrium line coincides with the line $P(\text{GPa}) = -4.7 \times T(\text{K}) + 3.14$, that was recommended by Essene [11] (Figure 6). At higher pressures, breyite transforms to the two-phase assembly of larnite (Ca_2SiO_4) and $CaSi_2O_5$ [1]. Based on this phase transition, the sum of the Gibbs energy of both phases is calculated. The phase boundary of breyite–(larnite + $CaSi_2O_5$) is calculated from equation 3Brt = β-Lrn + $CaSi_2O_5$ [12,57], using equilibrium of the Gibbs energy of breyite, larnite and Ca-titanite. After that, we can estimate the Gibbs energy of Ca-perovskite and calculate the line of phase transition from equation β-Lrn + $CaSi_2O_5$ = 3Ca-Pv [12,57]. It should be noted that the position of the calculated equilibrium lines (breyite–(larnite + $CaSi_2O_5$) and (larnite + $CaSi_2O_5$)–Ca-perovskite) depends entirely on the choice of the primary experimental data, which have a very significant scatter (see Figure 6). We performed a calibration of the Gibbs energy of Ca-perovskite based on the thermochemical data from [12], because we consider these data to be the most reliable. The stability field of high-pressure Ca-silicates were studied by [71,72] and significant deviations were determined. Thus, the obtained phase diagram of the $CaSiO_3$ system is based on modern *P-V-T* measurements for Ca-silicates and clarifies the phase boundaries under upper mantle conditions at the depth up to ~600 km.

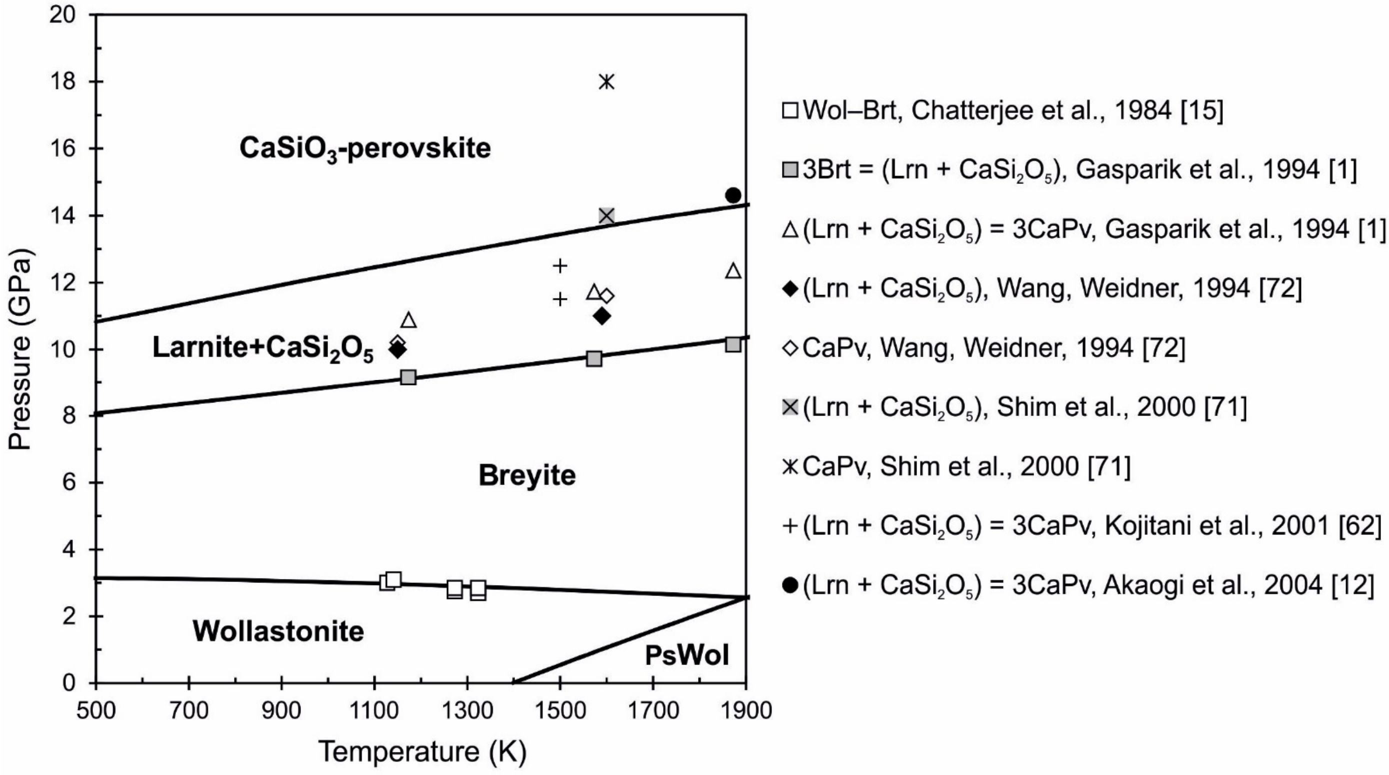

Figure 6. Calculated phase diagram of the $CaSiO_3$ system under upper mantle *P-T* conditions. Thick black lines are our calculations, symbols show the different experimental studies. The phase equilibria in the $CaSiO_3$ system were studied in [1,12,15,62] and stability field of mineral association (Lrn + $CaSi_2O_5$) and Ca-perovskite in [71,72].

There are many first-principles calculations based on density functional theory (DFT) for $CaSiO_3$-perovskite [73–76], however some of these were made at zero temperature [75,76].

The equation of state of $CaSiO_3$-perovskite based on ab initio molecular dynamic (AIMD) simulations was constructed in [74]. The authors believe that tetragonal structure of Ca-perovskite is stable at temperature range 1000–4000 K and pressure range 15–130 GPa. However, this assumption does not agree well with the melting line calculations in the $CaSiO_3$ system (see Figure 7). First-principle molecular dynamics calculations to investigate the structure of Ca-perovskite at high temperatures and pressures were made in [77]. The cubic structure of $CaSiO_3$-perovskite was found to be stable at temperatures higher 1000 K and at all pressures according to [77]. The phase boundaries in Ca-perovskite based on LDA and GGA approximations were calculated by Stixrude et al. [73]. The location of the phase transition from tetragonal to cubic structure in Ca-perovskite is shown in Figure 7. The gray area indicates the stability field of the tetragonal structure of Ca-perovskite according to [73,77].

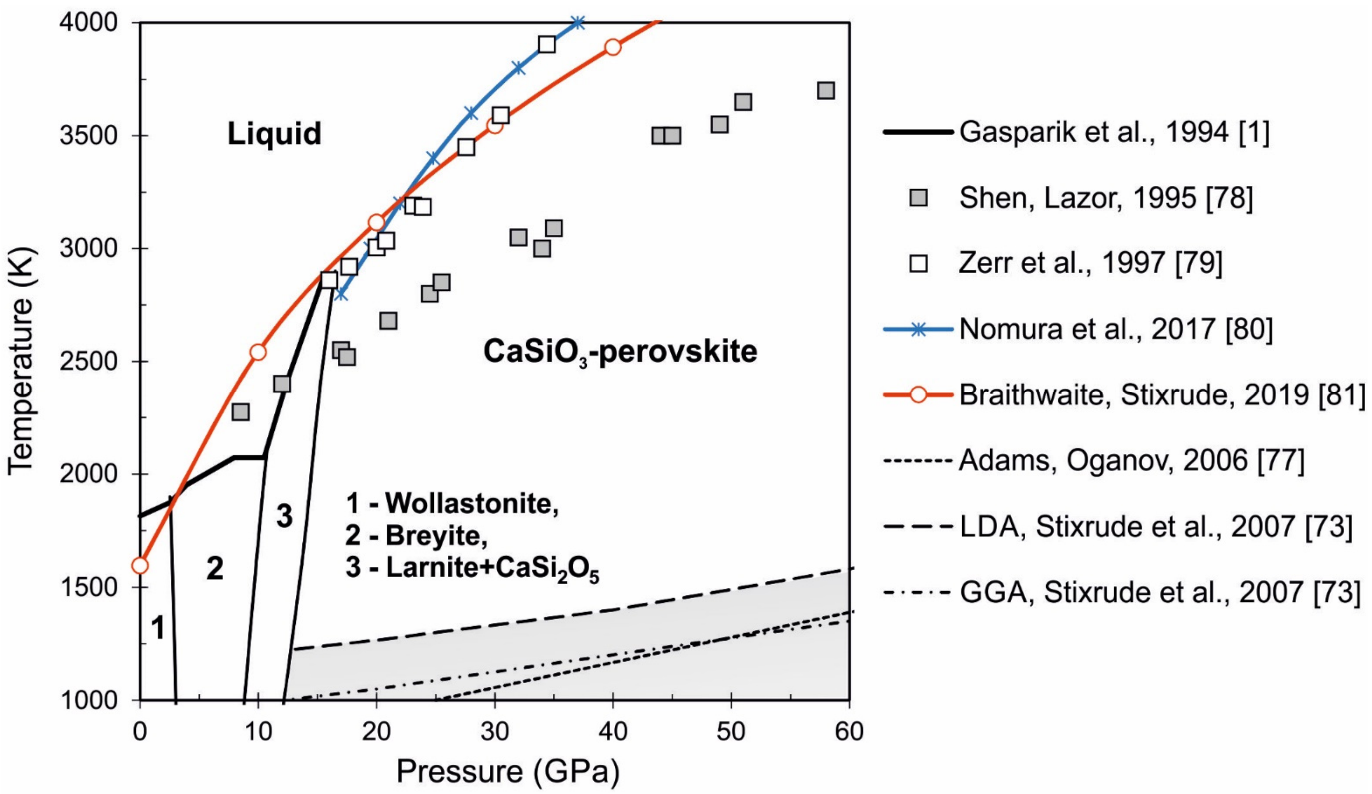

Figure 7. Phase diagram of the $CaSiO_3$ system under lower mantle *P-T* conditions. Thick black line, symbols, and color lines show melting line calculations from [1,78–81]; different dotted lines represent first-principle calculations of the phase boundaries in Ca-perovskite [73,77]. The gray area indicates the stability field of the tetragonal structure of Ca-perovskite.

The melting line in the $CaSiO_3$ system was studied experimentally at pressure up to 58 GPa in [1,78,79] and based on first-principles calculations in [80,81]. Figure 7 shows the comparison of the experimental data and different calculations. As can be seen, the experimental data from [79] are in good agreement with calculations [80,81] at the temperature range 2750–3500 K and at the pressure range 15–30 GPa. The melting line from [78] is lower than other estimates and difference increases at high pressures. The melting of $CaSiO_3$-perovskite is predicted in the range of very high temperatures and pressures up to 6400 K and 300 GPa, respectively, according to the recent study [81]. The melting temperature of $CaSiO_3$-perovskite significantly increases with pressure and is higher than that of $MgSiO_3$-perovskite.

The proposed equation of state of Ca-perovskite is of great interest for deep mineralogy. The thermodynamic parameters of the Earth's lower mantle can be estimated using the equation of state of Ca-perovskite. Table 4 shows the parameters of the Earth's lower mantle according to the PREM model (Preliminary Reference Earth Model) [82], where temperature is calculated from [83]. We calculated the density and adiabatic bulk modulus of $CaSiO_3$-perovskite at these *P*-*T* parameters (from Table 4) and compared it with the PREM model and with the density and adiabatic bulk modulus of $MgSiO_3$-perovskite from our previous study [16] (Figure 8). It can be seen that the density of Ca-perovskite is higher than the density of Mg-perovskite by about 0.1–0.15 gcm^{-3} and almost coincides with the density according to the PREM model (Figure 8a). The adiabatic bulk moduli of Ca-perovskite and Mg-perovskite differs slightly. However, with increasing pressure, adiabatic bulk modulus of $CaSiO_3$-perovskite exceeds the PREM model by 40 GPa at pressures of 120–130 GPa (Figure 8b). Moreover, we added the first-principle calculated data for the density and adiabatic bulk modulus of Ca-perovskite according to Li et al. [74]. The calculated density from [74] and calculated density from our equation of state for $CaSiO_3$-perovskite are very similar, especially in the high pressure range above 80 GPa (Figure 8a). The calculated values of the adiabatic bulk modulus are in less agreement (Figure 8b).

Table 4. Density and adiabatic bulk modulus of cubic $CaSiO_3$-perovskite at temperature, pressure, and depth of the lower mantle from the Preliminary Reference Earth Model (PREM) model.

Depth, km	*P*, GPa	*T*, K	Density, gcm^{-3}	*Ks*, GPa
2891	135.75	3739	5.483	686.56
2771	128.71	2838	5.499	673.01
2741	126.97	2740	5.492	668.35
2571	117.35	2668	5.412	637.46
2371	106.39	2596	5.317	601.82
2171	95.76	2525	5.220	566.86
1971	85.43	2452	5.122	532.51
1771	75.36	2379	5.022	498.60
1571	65.52	2302	4.920	465.04
1371	55.9	2227	4.814	431.71
1171	46.46	2144	4.705	398.53
971	37.29	2060	4.592	365.70
771	28.29	1974	4.474	332.80
670	23.83	1931	4.412	316.19

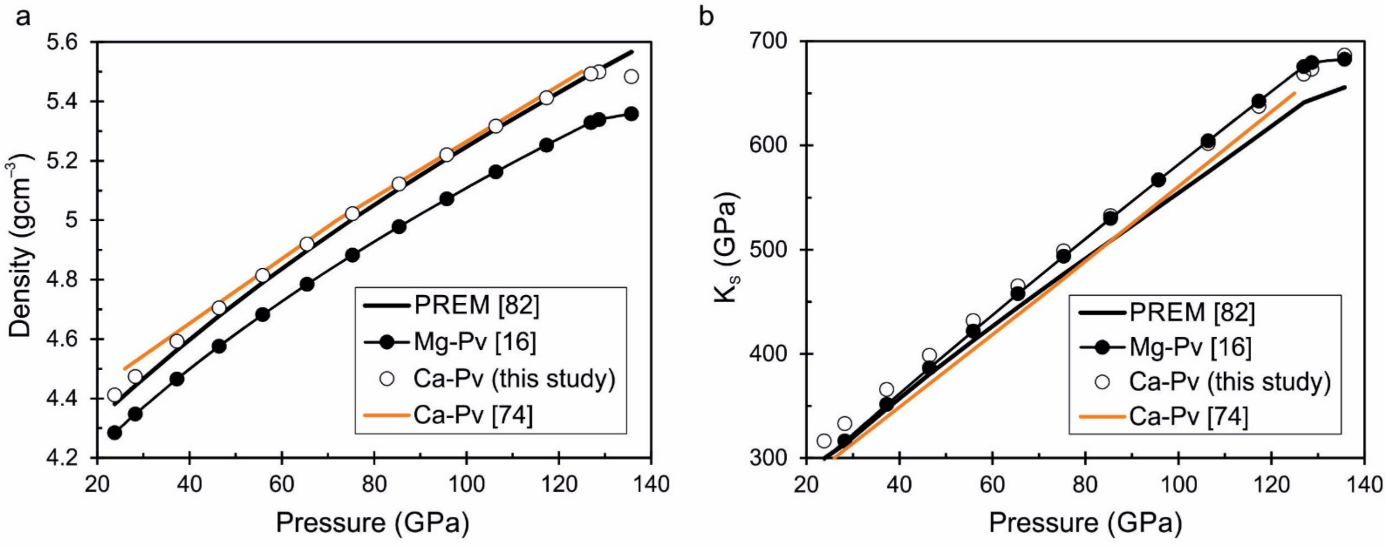

Figure 8. Densities (**a**) and adiabatic bulk moduli (**b**) of $MgSiO_3$-perovskite from [16] and $CaSiO_3$-perovskite from the present equation of state are calculated from the mantle geotherm in comparison with the density and adiabatic bulk modulus according to the PREM model [82] and calculation from [74].

Thus, the obtained results of the present study can be used to interpret of the phase and seismic boundaries in the Earth's upper mantle. Since calcium is one of the main components of the Earth's mantle, it has its influence on the location of the observed seismic boundaries. At a depth of about ~350 km, $CaSiO_3$ phase is contained as a component of clinopyroxene minerals, whereas below 350 km, it is concentrated as a component of complex garnet solid solutions (majorite garnet) [9,59]. The phase of $CaSiO_3$-perovskite is stabilized at increasing pressure and is considered one of the main minerals of the lower mantle, comprising up to 7 wt.% of peridotitic mantle, according to the modern geophysical data [84]. There is the view that the transition of the $CaSiO_3$ component in the garnet solid solution to form denser of Ca-perovskite is associated with seismic discontinuity at a depth of 520 km [59]. The phase transition of wadsleyite–ringwoodite in the Mg_2SiO_4 system also occurs at this depth at pressure 17–18 GPa, but it is characterized by a slight increase in density and adiabatic bulk modulus as was calculated and shown in our earlier study [16]. Accordingly, the phase transition in olivine cannot fully explain the seismic boundary at 520 km. Moreover, the olivine–wadsleyite transition at the depth 410 km at 14–15 GPa calculated in [16] corresponded to a temperature of ~1700 K [16], but according to the estimations in [85], the temperature in this depth is 1790 to 1830 K. The calculated phase transition of (larnite + $CaSi_2O_5$)–Ca-perovskite occurs at a depth of 410 km at temperatures 1700–1800 K (Figure 6). Although the phase transitions in the $CaSiO_3$ system cannot be directly responsible for the seismic boundaries in the upper mantle, they have an effect on the location of discontinuities and point to the role of calcium-containing minerals in the upper mantle.

It is well known that magnesium is the most abundant element in mantle minerals, but the ratios of main elements Mg, Fe, Ca, and Al remain an open question. The calculated density of $MgSiO_3$-perovskite from the mantle geotherm [83] is too low with respect to the PREM model. However, the calculated density of $CaSiO_3$-perovskite is in good agreement with the density by the PREM model (Figure 8a). The calcium content in the perovskite composition will increase the density of mineral, as well as the presence of iron. Such a composition will obviously be close to the real composition of the mantle material. The obtained thermodynamic data in the present study can be used in the calculation of silicate mixtures of different compositions, as was done for example in [86]. Thus, the possibilities of thermodynamic modeling for future calculations and investigation of deep mineralogy in the area that is not available for direct experimentation are opened.

5. Conclusions

We have constructed the equations of state of wollastonite, pseudowollastonite, breyite, larnite (Ca_2SiO_4), titanite-structured $CaSi_2O_5$ and $CaSiO_3$-perovskite using a thermodynamic model based on the Helmholtz free energy. The proposed equations of state are developed based on optimization of different experimental measurements at ambient conditions and to a high temperatures and pressures. The full set of thermodynamic properties (volume, thermal expansion, entropy, isobaric and isochoric heat capacity, bulk moduli, Gibbs energy, etc.) of studied Ca-silicates is calculated at given pressures and temperatures and is presented in the form of Tables to the present article. The calculated properties are compared with reference and experimental data. It is shown that the proposed equations of state reliably describe properties of studied Ca-silicates in a wide range of pressures and temperatures.

The phase diagram of the $CaSiO_3$ system is constructed at pressures up to 20 GPa and temperatures up to 2000 K. The calculated phase diagram are compared with experimental data for different phases and clarifies the phase boundaries in the $CaSiO_3$ system under upper mantle conditions. The phase transition of majorite garnet, which contains $CaSiO_3$ phase in its composition, to Ca-perovskite is associated with seismic boundary at the depth 520 km; therefore, it points to the role of calcium-containing minerals in the upper mantle region. The calculated density of $CaSiO_3$-perovskite is in good agreement with the density according to the PREM model at the lower-mantle region. The calculated thermodynamic data for Ca-perovskite open the possibilities of thermodynamic modeling at high pressures and temperatures.

Supplementary Materials: The following are available online at https://www.mdpi.com/2075-163X/11/3/322/s1, File S1: MS Excel spreadsheet for wollastonite (Wol.xls), File S2: MS Excel spreadsheet for pseudowollastonite (PsWol.xls), File S3: MS Excel spreadsheet for breyite (Brt.xls), File S4: MS Excel spreadsheet for larnite (Lrn.xls), File S5: MS Excel spreadsheet for titanite-structured $CaSi_2O_5$ (CaTit.xls), File S6: MS Excel spreadsheet for $CaSiO_3$-perovskite (CaPv.xls); Table S1: Thermodynamic functions of pseudowollastonite at different pressures and temperatures, Table S2: Thermodynamic functions of breyite at different pressures and temperatures, Table S3: Thermodynamic functions of larnite (Ca_2SiO_4) at different pressures and temperatures, Table S4: Thermodynamic functions of titanite-structured $CaSi_2O_5$ at different pressures and temperatures, Table S5: Thermodynamic functions of cubic $CaSiO_3$-perovskite at different pressures and temperatures.

Author Contributions: Conceptualization, T.S.S. and P.I.D.; methodology, P.I.D.; software, T.S.S.; writing—review and editing, T.S.S. and P.I.D.; visualization, T.S.S. and P.I.D.; supervision, P.I.D. All authors have read and agreed to the published version of the manuscript.

Funding: The study was supported by the Russian Science Foundation, grant No. 19-77-00031. The program used for calculation of thermodynamic functions of Ca-silicates in the present study was registered in the Russian Federation (certificate No. 2019610474).

Data Availability Statement: Data is contained within the article or supplementary material.

Acknowledgments: We would like to thank Igor S. Sharygin for valuable comments and the Reviewers for their constructive comments on this study. A detailed analysis of the present article by one of the Reviewers allowed us to significantly improve this manuscript.

Conflicts of Interest: The authors declare no conflict of interest.

References

1. Gasparik, T.; Wolf, K.; Smith, C.M. Experimental determination of phase relations in the $CaSiO_3$ system from 8 to 15 GPa. *Am. Mineral.* **1994**, *79*, 1219–1222.
2. Swamy, V.; Dubrovinsky, L.S. Thermodynamic data for the phases in the $CaSiO_3$ system. *Geochim. Cosmochim. Acta* **1997**, *61*, 1181–1191. [CrossRef]
3. Joswig, W.; Stachel, T.; Harris, J.W.; Baur, W.H.; Brey, G.P. New Ca-silicate inclusions in diamonds—Tracers from the lower mantle. *Earth Planet. Sci. Lett.* **1999**, *173*, 1–6. [CrossRef]
4. Stachel, T.; Harris, J.W.; Brey, G.P.; Joswig, W. Kankan diamonds (Guinea) II: Lower mantle inclusion parageneses. *Contrib. Mineral. Petrol.* **2000**, *140*, 16–27. [CrossRef]
5. Anzolini, C.; Angel, R.J.; Merlini, M.; Derzsi, M.; Tokar, K.; Milani, S.; Krebs, M.Y.; Brenker, F.E.; Nestola, F.; Harris, J.W. Depth of formation of $CaSiO_3$-walstromite included in super-deep diamonds. *Lithos* **2016**, *265*, 138–147. [CrossRef]
6. Nestola, F.; Korolev, N.; Kopylova, M.; Rotiroti, N.; Pearson, D.G.; Pamato, M.G.; Alvaro, M.; Peruzzo, L.; Gurney, J.J.; Moore, A.E.; et al. $CaSiO_3$ perovskite in diamond indicates the recycling of oceanic crust into the lower mantle. *Nature* **2018**, *555*, 237–241. [CrossRef]
7. Woodland, A.B.; Girnis, A.V.; Bulatov, V.K.; Brey, G.P.; Hofer, H.E. Breyite inclusions in diamond: Experimental evidence for possible dual origin. *Eur. J. Mineral.* **2020**, *32*, 171–185. [CrossRef]
8. Yang, H.; Prewitt, C.T. On the crystal structure of pseudowollastonite ($CaSiO_3$). *Am. Mineral.* **1999**, *84*, 929–932. [CrossRef]
9. Ringwood, A.E.; Major, A. Some high-pressure transformations of geophysical significance. *Earth Planet. Sci. Lett.* **1967**, *2*, 106–110. [CrossRef]
10. Brenker, F.; Nestola, F.; Brenker, L.; Peruzzo, L.; Secco, L.; Harris, J.W. Breyite, IMA 2018-062, CNMNC Newsletter. *Mineral. Mag.* **2018**, *82*, 1225–1232.
11. Essene, E. High-Pressure transformations in $CaSiO_3$. *Contrib. Mineral. Petrol.* **1974**, *45*, 247–250. [CrossRef]
12. Akaogi, M.; Yano, M.; Tejima, Y.; Iijima, M.; Kojitani, H. High-pressure transitions of diopside and wollastonite: Phase equilibria and thermochemistry of $CaMgSi_2O_6$, $CaSiO_3$ and $CaSi_2O_5$–$CaTiSiO_5$ system. *Phys. Earth Planet. Inter.* **2004**, *143–144*, 145–156. [CrossRef]
13. Kanazaki, M.; Stebbins, J.F.; Xue, X. Characterization of quenched high pressure phase in $CaSiO_3$ system by XRD and ^{29}Si NMR. *Geophys. Res. Lett.* **1991**, *18*, 463–466. [CrossRef]
14. Sueda, Y.; Irifune, T.; Yamada, A.; Inoue, T.; Liu, X.; Funakoshi, K. The phase boundary between $CaSiO_3$ perovskite and Ca_2SiO_4+$CaSi_2O_5$ determined by in situ X-ray observations. *Geophys. Res. Lett.* **2006**, *33*, L10307. [CrossRef]
15. Chatterjee, N.D.; Johannes, W.; Leistner, H. The system CaO-Al_2O_3-SiO_2-H_2O: New phase equilibria data, some calculated phase relations, and their petrological applications. *Contrib. Mineral. Petrol.* **1984**, *88*, 1–13. [CrossRef]

16. Dorogokupets, P.I.; Dymshits, A.M.; Sokolova, T.S.; Danilov, B.S.; Litasov, K.D. The equations of state of forsterite, wadsleyite, ringwoodite, akimotoite, $MgSiO_3$-perovskite, and postperovskite and phase diagram for the Mg_2SiO_4 system at pressures of up to 130 GPa. *Russ. Geol. Geophys.* **2015**, *56*, 172–189. [CrossRef]
17. Sokolova, T.S.; Dorogokupets, P.I.; Litasov, K.D.; Danilov, B.S.; Dymshits, A.M. Spreadsheets to calculate *P-V-T* relations, thermodynamic and thermoelastic properties of silicates in the $MgSiO_3$–MgO system. *High Press. Res.* **2018**, *38*, 193–211. [CrossRef]
18. Sokolova, T.S.; Dorogokupets, P.I.; Litasov, K.D. Self-consistent pressure scales based on the equations of state for ruby, diamond, MgO, B2–NaCl as well as Au, Pt, and other metals to 4 Mbar and 3000 K. *Russ. Geol. Geophys.* **2013**, *54*, 181–199. [CrossRef]
19. Sokolova, T.S.; Dorogokupets, P.I.; Dymshits, A.M.; Danilov, B.S.; Litasov, K.D. Microsoft excel spreadsheets to calculate *P-V-T* relations and thermodynamic properties from equations of state of nine metals, MgO and diamond used as pressure markers in high-pressure and high-temperature experiments. *Comput. Geosci.* **2016**, *94*, 162–169. [CrossRef]
20. Dorogokupets, P.I.; Dymshits, A.M.; Litasov, K.D.; Sokolova, T.S. Thermodynamics and equations of state of iron to 350 GPa and 6000 K. *Sci. Rep.* **2017**, *7*, 1–11. [CrossRef]
21. Litasov, K.D.; Sharygin, I.S.; Shatskii, A.F.; Gavryushkin, P.N.; Dorogokupets, P.I.; Sokolova, T.S.; Ohtani, E.; Dymshits, A.M.; Alifirova, T.A. *P–V–T* Equations of state for iron carbides Fe_3C and Fe_7C_3 and their relationships under the conditions of the Earth's mantle and core. *Dokl. Earth Sci.* **2013**, *453*, 1269–1273. [CrossRef]
22. Dorogokupets, P.I.; Sokolova, T.S.; Dymshits, A.M.; Litasov, K.D. Thermodynamic properties of rock-forming oxides, α-Al_2O_3, Cr_2O_3, α-Fe_2O_3, and Fe_3O_4 at high temperatures and pressures. *Geodynam. Tectonophys.* **2016**, *7*, 459–476. [CrossRef]
23. Magomedov, M.N. Variations in thermal properties of diamond under isothermal compression. *Tech. Phys.* **2017**, *62*, 661–668.
24. Angel, R.J.; Miozzi, F.; Alvaro, M. Limits to the validity of thermal-pressure equations of state. *Minerals* **2019**, *9*, 562. [CrossRef]
25. Katsura, T.; Tange, Y. A simple derivation of the Birch–Murnaghan equations of state (EOSs) and comparison with EOSs derived from other definitions of finite strain. *Minerals* **2019**, *9*, 745. [CrossRef]
26. Khishchenko, K.V. Equation of state for rhenium at high pressures. *J. Phys. Conf. Ser.* **2020**, *1556*, 012041. [CrossRef]
27. Zharkov, V.N.; Kalinin, V.A. *Equations of State for Solids at High Pressures and Temperatures*; Consuitants Bureau: New York, NY, USA, 1971.
28. Kunc, K.; Loa, I.; Syassen, K. Equation of state and phonon frequency calculations of diamond at high pressures. *Phys. Rev. B* **2003**, *68*, 094107. [CrossRef]
29. Vinet, P.; Ferrante, J.; Rose, J.H.; Smith, J.R. Compressibility of solids. *J. Geophys. Res.* **1987**, *92*, 9319–9325. [CrossRef]
30. Holzapfel, W.B. Physics of solids under strong compression. *Rep. Prog. Phys.* **1996**, *59*, 29–90. [CrossRef]
31. Birch, F. Finite strain isotherm and velocities for single-crystal and polycrystalline NaCl at high pressures and 300 K. *J. Geophys. Res. Solid Earth* **1978**, *83*, 1257–1268. [CrossRef]
32. Dorogokupets, P.I.; Oganov, A.R. Equations of state of Al, Au, Cu, Pt, Ta, and W and revised ruby pressure scale. *Dokl. Earth Sci.* **2006**, *410*, 1091–1095. [CrossRef]
33. Dorogokupets, P.I.; Oganov, A.R. Ruby, metals, and MgO as alternative pressure scales: A semiempirical description of shock-wave, ultrasonic, X-ray, and thermochemical data at high temperatures and pressures. *Phys. Rev. B* **2007**, *75*, 024115. [CrossRef]
34. Al'tshuler, L.V.; Brusnikin, S.E.; Kuz'menkov, E.A. Isotherms and Gruneisen functions of 25 metals. *J. Appl. Mech. Tech. Phys.* **1987**, *28*, 129–141. [CrossRef]
35. Schmetterer, C.; Masset, P.J. Heat capacity of compounds in the CaO-SiO_2 System—A Review. *J. Phase Equilib. Diffus.* **2012**, *33*, 261–275. [CrossRef]
36. Swamy, V.; Dubrovinsky, L.S.; Tutti, F. High-temperature Raman spectra and thermal expansion of wollastonite. *J. Am. Ceram. Soc.* **1997**, *80*, 2237–2247. [CrossRef]
37. Vaiday, S.N.; Bailey, S.; Pasternack, T.; Kennedy, G.C. Compressibility of fifteen minerals to 45 kilobars. *J. Geophys. Res.* **1973**, *78*, 6893–6898. [CrossRef]
38. Yang, H.; Prewitt, C.T. Crystal structure and compressibility of a two-layer polytype of pseudowollastonite ($CaSiO_3$). *Am. Mineral.* **1999**, *84*, 1902–1905. [CrossRef]
39. Southard, J.C. A modified calorimeter for high temperatures. The heat content of silica, wollastonite and thorium dioxide above 25°. *J. Am. Chem. Soc.* **1941**, *63*, 3142–3146. [CrossRef]
40. Krupka, K.M.; Robie, R.A.; Hemingway, B.S.; Kerrick, D.M. Low-temperature heat capacities an derived thermodynamic properties of anthophyllite, diopside, enstatite, bronzite, and wollastonite. *Am. Mineral.* **1985**, *70*, 249–260.
41. Krupka, K.M.; Robie, R.A.; Hemingway, B.S.; Kerrick, D.M. High-temperature heat capacities and derived thermodynamic properties of anthophyllite, diopside, dolomite, enstatite, bronzite, talc, tremolite, and wollastonite. *Am. Mineral.* **1985**, *70*, 261–271.
42. Richet, P.; Fiquet, G. High-Temperature heat capacity and premelting of minerals in the system MgO-CaO-Al_2O_3-SiO_2. *J. Geophys. Res.* **1991**, *96*, 445–456. [CrossRef]
43. Holland, T.J.B.; Powell, R. An improved and extended internally consistent thermodynamic dataset for phases of petrological interest, involving a new equation of state for solids. *J. Metamorph. Geol.* **2011**, *29*, 333–383. [CrossRef]
44. Richet, P.; Mysen, B.O.; Ingrib, J. High-temperature X-ray diffraction and Raman spectroscopy of diopside and pseudowollastonite. *Phys. Chem. Miner.* **1998**, *25*, 401–414. [CrossRef]
45. White, W.P. Silicate specific heats, Second series. *Am. J. Sci.* **1919**, *47*, 1–44. [CrossRef]

46. Parks, G.S.; Kelley, K.K. The heat capacity of calcium silicate. *J. Phys. Chem.* **1926**, *30*, 1175–1178. [CrossRef]
47. Berman, R.G.; Brown, T.H. Heat capacity of minerals in the system Na_2O-K_2O-CaO-MgO-FeO-Fe_2O_3-$A1_2O_3$-SiO_2-TiO_2-H_2O-CO_2: Representation, estimation, and high temperature extrapolation. *Contrib. Mineral. Petrol.* **1985**, *89*, 168–183. [CrossRef]
48. Huang, W.-L.; Wyllie, P.J. Melting and subsolidus phase relationships for $CaSiO_3$ to 35 kilobars pressure. *Am. Mineral.* **1975**, *60*, 213–217.
49. Joswig, W.; Paulus, E.F.; Winkler, B.; Milman, V. The crystal structure of $CaSiO_3$-walstromite, a special isomorph of wollastonite-II. *Z. Krist.* **2003**, *218*, 811–818. [CrossRef]
50. Liu, X.; Wang, S.; He, Q.; Chen, J.; Wang, H.; Li, S.; Peng, F.; Zhang, L.; Fei, Y. Thermal elastic behavior of $CaSiO_3$-walstromite: A powder X-ray diffraction study up to 900 °C. *Am. Mineral.* **2012**, *97*, 262–267. [CrossRef]
51. Remy, C.; Andrault, D.; Madon, M. High-temperature, high-pressure X-ray investigation of dicalcium silicate. *J. Am. Ceram. Soc.* **1997**, *80*, 851–860. [CrossRef]
52. Yamnova, N.A.; Zubkova, N.V.; Eremin, N.N.; Zadov, A.E.; Gazeev, V.M. Crystal structure of larnite β-Ca_2SiO_4 and specific features of polymorphic transitions in dicalcium orthosilicate. *Crystallogr. Rep.* **2011**, *56*, 210–220. [CrossRef]
53. Tilley, C.E. On larnite (calcium orthosilicate, a new mineral) and its associated minerals from the limestone contact-zone of Scawt Hill, Co. Antrim. *Mineral. Mag.* **1929**, *22*, 77–86. [CrossRef]
54. Todd, S.S. Low-temperature heat capacities and entropies at 298.16 °K of crystalline calcium orthosilicate, zinc orthosilicate and tricalcium silicate. *J. Am. Chem. Soc.* **1951**, *73*, 3277–3278. [CrossRef]
55. Coughlin, J.P.; O'Brien, C.J. High temperature heat contents of calcium orthosilicate. *J. Phys. Chem.* **1957**, *61*, 767–769. [CrossRef]
56. Fukuda, K.; Maki, I.; Ito, S. Anisotropic thermal expansion of β-Ca_2SiO_4 monoclinic crystal. *J. Am. Ceram. Soc.* **1997**, *80*, 1595–1598. [CrossRef]
57. Xiong, Z.; Liu, X.; Shieh, S.R.; Wang, S.; Chang, L.; Tang, J.; Hong, X.; Zhang, Z.; Wang, H. Some thermodynamic properties of larnite (β-Ca_2SiO_4) constrained by high *T/P* experiment and/or theoretical simulation. *Am. Miner.* **2016**, *101*, 277–288. [CrossRef]
58. Angel, R.J.; Kunz, M.; Miletich, R.; Woodland, A.B.; Koch, M.; Knoche, R.L. Effect of isovalent Si, Ti substitution on the bulk moduli of $Ca(Ti_{1\text{-}x}Si_x)SiO_5$ titanites. *Am. Miner.* **1999**, *84*, 282–287. [CrossRef]
59. Ringwood, A.E.; Major, A. Synthesis of majorite and other high pressure garnets and perovskites. *Earth Planet. Sci. Lett.* **1971**, *12*, 411–418. [CrossRef]
60. Sun, N.; Mao, Z.; Yan, S.; Wu, X.; Prakapenka, V.B.; Lin, J.-F. Confirming a pyrolitic lower mantle using self-consistent pressure scales and new constraints on $CaSiO_3$ perovskite. *Phys. Res. Solid Earth* **2016**, *121*, 4876–4894. [CrossRef]
61. Chen, H.; Shim, S.-H.; Leinenweber, K.; Prakapenka, V.; Meng, Y.; Prescher, C. Crystal structure of $CaSiO_3$ perovskite at 28–62 GPa and 300 K under quasi-hydrostatic stress conditions. *Am. Miner.* **2018**, *103*, 462–468. [CrossRef]
62. Kojitani, H.; Navrotsky, A.; Akaogi, M. Calorimetric study of perovskite solid solutions in the $CaSiO_3$-$CaGeO_3$ system. *Phys. Chem. Miner.* **2001**, *28*, 413–420. [CrossRef]
63. Noguchi, M.; Komabayashi, T.; Hirose, K.; Ohishi, Y. High-temperature compression experiments of $CaSiO_3$ perovskite to lowermost mantle conditions and its thermal equation of state. *Phys. Chem. Miner.* **2013**, *40*, 81–91. [CrossRef]
64. Greaux, S.; Irifune, T.; Higo, Y.; Tange, Y.; Arimoto, T.; Liu, Z.; Yamada, A. Sound velocity of $CaSiO_3$ perovskite suggests the presence of basaltic crust in the Earth's lower mantle. *Nature* **2019**, *565*, 218–221. [CrossRef]
65. Dorogokupets, P.I.; Dewaele, A. Equations of state of MgO, Au, Pt, NaCl-B1, and NaCl-B2: Internally consistent high-temperature pressure scales. *High Press. Res.* **2007**, *27*, 431–446. [CrossRef]
66. Fei, Y.W.; Ricolleau, A.; Frank, M.; Mibe, K.; Shen, G.Y.; Prakapenka, V. Toward an internally consistent pressure scale. *Proc. Natl. Acad. Sci. USA* **2007**, *104*, 9182–9186. [CrossRef] [PubMed]
67. Matsui, M.; Higo, Y.; Okamoto, Y.; Irifune, T.; Funakoshi, K.I. Simultaneous sound velocity and density measurements of NaCl at high temperatures and pressures: Application as a primary pressure standard. *Am. Miner.* **2012**, *97*, 1670–1675. [CrossRef]
68. Mao, H.K.; Chen, L.C.; Hemley, R.J.; Jephcoat, A.P.; Wu, Y. Stability and equation of state of $CaSiO_3$-perovskite to 134 GPa. *J. Geophys. Res.* **1989**, *94*, 17889–17894. [CrossRef]
69. Shim, S.-H.; Duffy, T.S.; Shen, G. The equation of state of $CaSiO_3$ perovskite to 108 GPa at 300 K. *Phys. Earth Planet. Inter.* **2000**, *120*, 327–338. [CrossRef]
70. Wang, Y.; Weidner, D.J.; Guyot, F. Thermal equation of state of $CaSiO_3$ perovskite. *J. Geophys. Res.* **1996**, *101*, 661–672. [CrossRef]
71. Shim, S.-H.; Duffy, T.; Shen, G. The stability and P-V-T equation of state of $CaSiO_3$ perovskite in the Earth's lower mantle. *J. Geophys. Res.* **2000**, *105*, 25955–25968. [CrossRef]
72. Wang, Y.; Weidner, D.J. Thermoelasticity of $CaSiO_3$ perovskite and implications for the lower mantle. *Geophys. Res. Lett.* **1994**, *21*, 895–898. [CrossRef]
73. Stixrude, L.; Lithgow-Bertelloni, C.; Kiefer, B.; Fumagalli, P. Phase stability and shear softening in $CaSiO_3$ perovskite at high pressure. *Phys. Rew. B* **2007**, *75*, 024108. [CrossRef]
74. Li, L.; Weidner, D.J.; Brodholt, J.; Alfe, D.; Price, G.D.; Caracas, R.; Wentzcovitch, R. Elasticity of $CaSiO_3$ perovskite at high pressure and high temperature. *Phys. Earth Planet. Inter.* **2006**, *155*, 249–259. [CrossRef]
75. Caracas, R.; Wentzcovitch, R.; Price, G.D.; Brodholt, J. $CaSiO_3$ perovskite at lower mantle pressures. *Geophys. Res. Lett.* **2005**, *32*, L06306. [CrossRef]
76. Karki, B.B.; Crain, J. First-principles determination of elastic properties of $CaSiO_3$ perovskite at lower mantle pressures. *Geophys. Res. Lett.* **1998**, *25*, 2741–2744. [CrossRef]

77. Adams, D.J.; Oganov, A. Ab initio molecular dynamics study of $CaSiO_3$ perovskite at *P-T* conditions of Earth's lower mantle. *Phys. Rev. B* **2006**, *73*, 184106. [CrossRef]
78. Shen, G.; Lazor, P. Measurement of melting temperatures of some minerals under lower mantle pressures. *J. Geophys. Res.* **1995**, *100*, 17699–17713. [CrossRef]
79. Zerr, A.; Serghiou, G.; Boehler, R. Melting of $CaSiO_3$ perovskite to 430 kbar and first *in-situ* measurements of lower mantle eutectic temperatures. *Geophys. Res. Lett.* **1997**, *24*, 909–912. [CrossRef]
80. Nomura, R.; Zhou, Y.; Irifune, T. Melting phase relations in the $MgSiO_3$–$CaSiO_3$ system at 24 GPa. *Prog. Earth Planet. Sci.* **2017**, *4*, 1–11. [CrossRef]
81. Braithwaite, J.; Stixrude, L. Melting of $CaSiO_3$ perovskite at high pressure. *Geophys. Res. Lett.* **2019**, *46*, 2037–2044. [CrossRef] [PubMed]
82. Dziewonski, A.; Anderson, D. Preliminary reference Earth model. *Phys. Earth Planet. Inter.* **1981**, *25*, 297–356. [CrossRef]
83. Stacey, F.D.; Davis, P.M. High pressure equations of state with applications to the lower mantle and core. *Phys. Earth Planet. Inter.* **2004**, *142*, 137–184. [CrossRef]
84. Irifune, T.; Shinmei, T.; McCammon, C.A.; Miyajima, N.; Rubie, D.C.; Frost, D.J. Iron partitioning and density changes of pyrolite in Earth's lower mantle. *Science* **2010**, *327*, 193–195. [CrossRef] [PubMed]
85. Katsura, T.; Yoneda, A.; Yamazaki, D.; Yoshino, T.; Ito, E. Adiabatic temperature profile in the mantle. *Phys. Earth Planet. Inter.* **2010**, *183*, 212–218. [CrossRef]
86. Sokolova, T.S.; Seredkina, A.I.; Dorogokupets, P.I. Density patterns of the upper mantle under Asia and the Arctic: Comparison of thermodynamic modeling and geophysical data. *Pure Appl. Geophys.* **2020**, *177*, 4289–4307. [CrossRef]